

# 3D reconstruction of external and internal surfaces of transparent objects from polarization state of highlights

Florence Drouet,\* Christophe Stolz, Olivier Laligant, and Olivier Aubreton

Université de Bourgogne Le2i, UMR CNRS 6306, allée Alain Savary, Dijon 21000, France

\*Corresponding author: [florence.drouet@u-bourgogne.fr](mailto:florence.drouet@u-bourgogne.fr)

Received February 25, 2014; revised April 11, 2014; accepted April 12, 2014;  
posted April 14, 2014 (Doc. ID 207092); published 0 MONTH 0000

A vision-based method is proposed to measure the 3D shape of external and internal surfaces (not accessible) of smooth transparent objects. Looking at the reflections of point sources on a specular surface with a polarimetric camera, we combine the measurements of two techniques: shape from distortion and shape from polarization. It permits us to recover the position and orientation of the specular surface for each detected point. The internal surface of transparent objects exhibiting as well a specular component, the same technique is used on the highlights coming from the back surface, taking into account the refraction by using polarimetric ray tracing. © 2014 Optical Society of America

OCIS codes: (150.6910) Three-dimensional sensing; (110.5405) Polarimetric imaging.  
<http://dx.doi.org/10.1364/OL.99.099999>

The 3D reconstruction of transparent objects is still an open problem in computer vision as shown in the state of the art of Ihrke *et al.* [1]. Transparent surfaces often have a partial specular behavior, so techniques developed to acquire purely specular objects can be used to get the external shape; for example, a shape from distortion techniques [2,3], polarization [4,5], or scatter-trace photography [6]. Several methods aim at reconstructing completely transparent objects, with both internal and external shapes—light field distortion [7], direct ray measurement [8], and tomography [9]—by immersing the object into a fluorescent fluid [10] or by using motion [11]. Those techniques rely on light transmission rather than reflection. In fact, the internal surface of transparent objects presents as well as the external one a partial specular behavior. The approach in this Letter is developed for nonaccessible internal surfaces of transparent objects. It relies on specular measurement technique. We focus on locally planar surfaces, and we tackle the extension to more general surfaces with first results on cylindrical surfaces.

Figure 1 illustrates the observation of one pattern reflected from both faces of a transparent object. One part of light is reflected on the external surface, at point  $P_1$ . Another part is first transmitted at point  $I$ , then reflected on the back surface, and transmitted again at point  $J$  [Fig. 1(a)]. These two light paths create an overlapped image. For example, the two reflections of a grid pattern on a transparent plate can be seen Fig. 1(b). With a dense pattern, or global illumination, these two reflections would be superimposed, making the measurement difficult. The idea is then to use a sparse set of illumination points, so that the reflections are more likely to be separated in the image. But with sparse data, most of the current techniques used to scan specular surfaces cannot be applied.

For example, a shape from distortion techniques consists in looking at the reflection of a known point source  $S$  on a specular surface with a calibrated camera. The surface must lie on the reflected line  $\vec{r}_1$  [Fig. 2(a)]. This ray and the point source  $S$  define a plane  $\Pi_1$ , which is the

incidence plane. The reflection determines the depth  $d_1$  and the surface normal  $\vec{n}_1$  only up to a 1D family of solution [12]: the knowledge of the normal gives the distance and the other way round. Usually, this ambiguity is lifted with optimization and integration [1], but this cannot be applied with sparse point source.

Therefore the shape from polarization technique consists in computing the normal map of the observed specular surface by measuring the polarization state of the light reflected from the surface, assuming prior knowledge of the refraction index  $n$ . The Stokes vector of the observed light is calculated as follows:

$$S_{1r} = C(\varphi)R_{1 \rightarrow n}(\theta_{1r})C(-\varphi)S_i, \quad (1)$$

with  $S_i = (1, 0, 0, 0)^T$  the incident Stokes vector, corresponding to unpolarized light.  $C$  is the Mueller rotation matrix, and  $\varphi$  is the angle between the world coordinate system and the coordinate system of the plane  $\Pi_1$ .  $R$  is the Mueller reflection matrix [13], which depends on the incident angle  $\theta_{1r}$ . We denote  $R_{1 \rightarrow n}$  because the light is going from the medium with index of refraction 1 (air) to the transparent medium with index  $n$ . The result of Eq. (1) corresponds to a light that is partially linearly

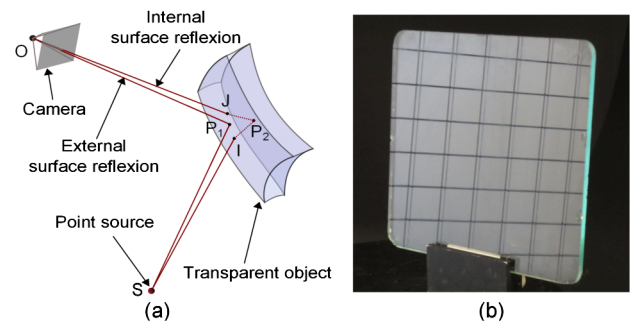


Fig. 1. Specular behavior of the two surfaces of a transparent object. (a) Ray tracing for the reflection of a point source. (b) Observation of the reflections of a regular grid on a transparent planar plate.

polarized, perpendicularly to the plane of incidence  $\Pi_1$ . The ellipticity being equal to zero, a polarizer with at least three orientations (partial Stokes polarimeter) is sufficient to measure the polarization state [14]. The degree of polarization of the reflected light is directly related to the angle of incidence [Fig. 2(b)]. Given the measured degree  $\rho_{1M}$ , there are two possible angles  $\theta_{1r}$ . Some means exist to lift this ambiguity [15], but in our case incidence angles are supposed to be inferior to the Brewster angle  $\theta_{Be}$ . The angle of polarization is directly linked with the orientation of the plane of incidence  $\Pi_1$ . Then the measurements  $\rho_{1M}$  and  $\varphi$  enable us to compute the surface normal  $\vec{n}_1$  at the incidence point  $P_1$ .

Our method consists in combining the results of those two methods. The shape from distortion gives the orientation position ambiguity, and the degree of polarization of the reflection  $\rho_{1M}$  lifts this ambiguity. We can notice that the orientation of the incidence plane  $\Pi_1$  is entirely defined by the shape from distortion measurement, so the angle of polarization estimation gives redundant information.

Now we suppose that the shape and position of the external surface are estimated, and we suppose that this surface  $Sl$  is locally planar around the points  $I$ ,  $J$ , and  $P_1$ , (same normal  $\vec{n}_1$ ). This assumption is called the planar hypothesis, it is more and more crucial when the thickness of the object is increased (implying a larger distance  $IJ$  on external surface). In the image, the reflection coming from the internal surface enables to compute the ray  $\vec{r}_2$ . This ray intersects the local external surface  $Sl$  at point  $J$  [Fig. 3(a)]. The internal surface must lie on the refracted ray  $\vec{r}_{2t}$ . We studied the geometrical constraints between the position and orientation of this internal surface, taking into account the refraction.

First, we set the distance  $d_2$  of the point  $P_2$  along the ray  $\vec{r}_{2t}$ . Because of the refraction at point  $I$ , the path between  $S$  and  $P_2$  is no longer a straight line. The rays  $\vec{i}_2$  and  $\vec{i}_{2t}$  are unknown, as well as the point  $I$ , so the normal  $\vec{n}_2$  cannot be computed directly. The goal is to find the path of light between  $S$  and  $P_2$ , which is equivalent to find the point  $I$  position. This problem was addressed by Glaeser and Schröcker [16]. It can be simplified to a 1D problem by defining a new coordinate system, in an auxiliary plane  $\Pi_{2i}$  defined by the points  $S$ ,  $P_2$ , and the vector  $\vec{n}_1$  [Fig. 3(b)]. This plane is the plane of incidence of the first refraction occurring at  $I$ . The point  $I$  must lie on the line defined by  $y'$ . This problem involves the Fermat's principle, with path-time minimization. The

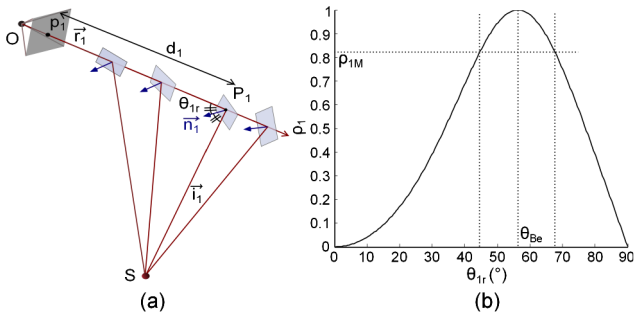


Fig. 2. (a) Shape from distortion ambiguity for the external surface. (b) Degree of polarization  $\rho_1$  as a function of the incidence angle on the external surface  $\theta_{1r}$ .

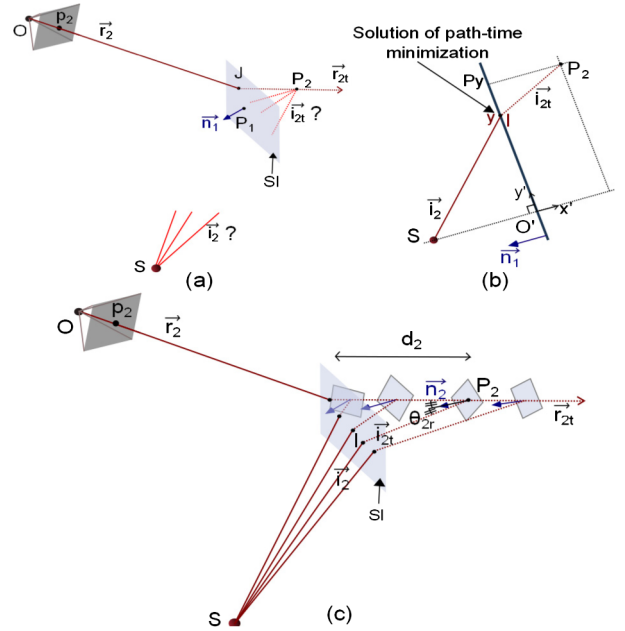


Fig. 3. Shape from distortion ambiguity for the internal surface. (a) Given the position of point  $P_2$  along the ray  $\vec{r}_{2t}$ , we cannot directly compute the normal  $\vec{n}_2$ , as we do not know either the ray  $\vec{i}_{2t}$  or  $\vec{i}_2$ . (b) Placing into the plane of incidence  $\Pi_{2i}$ , we can compute the path of light by using Fermat's principle. (c) Once the point  $I$  position is computed, it is possible to get the normal  $\vec{n}_2$ . The reverse, computation of  $P_2$  position from the normal  $\vec{n}_2$ , is straightforward using Snell's law and triangulation.

two authors showed that the solution is the root of a fourth-degree polynomial, and that it exists exactly at one root in the interval  $[0, Py]$ , which is the real solution. Once the point  $I$  is computed, it enables the computation of the ray  $\vec{i}_{2t}$ . Finally, the normal  $\vec{n}_2$  is then the bisector of the two rays  $\vec{r}_{2t}$  and  $\vec{i}_{2t}$ .

On the contrary, we set the normal  $\vec{n}_2$ . With the vectorial form of Snell's law, and the planar hypothesis, the vector  $\vec{i}_{2t}$  and then the vector  $\vec{i}_2$  are computed. Knowing the starting point of light  $S$ , the point  $P_2$  can be triangulated.

Finally, we showed that the shape from distortion technique applied to the internal surface presents the same position orientation ambiguity as for the external surface (assuming the planar hypothesis).

We also studied the shape from polarization method for the reflection coming from the internal surface. In the Mueller calculus, we have now to take into account one transmission (incident angle  $\theta_{2i}$ ), one reflection (incident angle  $\theta_{2r}$ ), and again one transmission (incident angle  $\theta_{2s}$ ). Between each reflection/transmission, a rotator Mueller matrix is applied in order to be in the reference system of the corresponding incident plane. In the general case, the three incidence planes are different. The resulting Stokes vector of the observed light is:

$$S_{2r} = C(\varphi_s)T_{n \rightarrow 1}(\theta_{2s})C(-\varphi_s) \\ \cdot C(\varphi_r)R_{n \rightarrow 1}(\theta_{2r})C(-\varphi_r) \\ \cdot C(\varphi_i)T_{1 \rightarrow n}(\theta_{2i})C(-\varphi_i)S_i. \quad (2)$$

We suppose that there is never total internal reflection. From Eq. (2), we can show easily that the fourth component of the Stokes vector is zero; hence the ellipticity is equal to zero, and the light is partially linearly polarized. Then the Stokes measurement requires the same setup as for the external surface (a partial Stokes polarimeter). The parameters  $\varphi_s$  and  $\theta_{2s}$  can be inferred by computing the point  $J$  intersection between the ray  $\vec{r}_2$  and the local external surface  $Sl$ . So we have here four unknowns, compared to only two for the external reflection. We were not able to split up the equations between the parameters  $\varphi$  and  $\theta$ , so we did not find how to directly measure the orientation of the normal  $\vec{n}_2$ .

But in the particular case when the three incidence planes are coplanar, several rotation matrices cancel each other out. Equation (2) becomes

$$S_{2r} = C(\varphi_s)T_{n \rightarrow 1}(\theta_{2s})R_{n \rightarrow 1}(\theta_{2r})T_{1 \rightarrow n}(\theta_{2i})C(-\varphi_i)S_i. \quad (3)$$

Neither  $C(-\varphi_i)$ , neither  $C(\varphi_s)$  play a role on the value of the degree of polarization. Figure 4(b) illustrates the geometrical constraints on the three incident angles. The points  $I$ ,  $J$ , and  $P_2$  form a triangle, making the angle  $\theta_{2i}$  directly linked with  $\theta_{2r}$ . The only remaining unknown is  $\theta_{2r}$ , and we can compute  $\rho_2$  as function of this variable [Fig. 4(a)]. We observe that the value of the parameter  $\theta_{2si}$  changes slightly the shape of this function. We applied several constraints on the angles values:  $\theta_{2r}$  and  $\theta_{2it}$  smaller than total reflection angle, and  $\beta$  smaller than  $90^\circ$ . We see that the resulting shape is similar to the shape on the function Fig. 2(b). Therefore the measurement  $\rho_{2M}$  permits to compute the angle of incidence  $\theta_{2r}$  (this angle is supposed to be inferior to the Brewster angle  $\theta_{Bi}$ ).

So the combination of the two techniques gives the same result as for the external surface in this coplanar case: given the reflected ray  $\vec{r}_2$ , and the measurement  $\rho_{2M}$ , it is possible to uniquely recover position and orientation of the internal surface.

In the general case, where the incidence planes are not necessarily equal, we propose to combine both techniques by computing the position of  $P_2$  with numerical optimization by finding the root of the equation:

$$f(d_2) = \rho_{2M} - \rho(d_2). \quad (4)$$

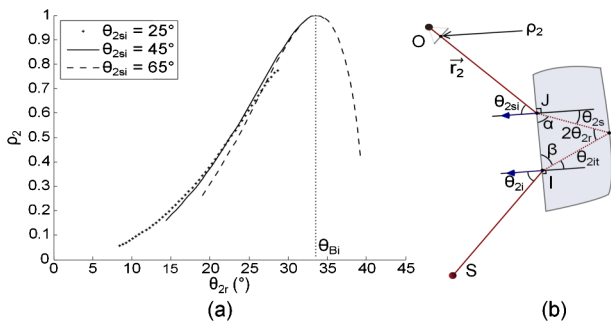


Fig. 4. Shape from polarization for the internal surface in the coplanar case. (a) Degree of polarization  $\rho_2$  as a function of the incident angle on the internal surface  $\theta_{2r}$ , for three values of  $\theta_{2si}$ . (b) Geometry in the coplanar case.

Given the distance  $d_2$  [Fig. 3(c)], we have already shown that it is possible to compute the point  $I$  position and then to get the whole light path. Then, by using Mueller calculus with Eq. (2), it is possible to simulate the degree of polarization  $\rho(d_2)$  associated with this distance  $d_2$ . The value  $d_2$ , for which the measured degree of polarization  $\rho_{2M}$  and the simulated one  $\rho_2$  are equal, corresponds to the actual distance of the point  $P_2$  along the ray  $\vec{r}_{2i}$ . So, in the general case, the measurement  $\rho_{2M}$  also enables us to lift the position orientation ambiguity.

Our algorithm is as follows. We suppose that the system is fully calibrated and that the medium is homogeneous, non-birefringent, with a known index of refraction  $n$ . We also suppose the planar hypothesis for the external surface.

- (1) Detection of the reflections of the point sources in the image. Association with one real point source, and association with external or internal surface
- (2) Measurement of  $\rho_{1M}$  and  $\rho_{2M}$
- (3) Computation of the rays  $\vec{r}_1$  and  $\vec{r}_2$
- (4) Computation of  $\theta_{1r}$  [Fig. 2(b)], and of the normal  $\vec{n}_1$
- (5) Computation of  $P_1$ , and of the local surface  $Sl$
- (6) Computation of the intersection  $J$  between ray  $\vec{r}_2$  and  $Sl$ , then computation of the refracted ray  $\vec{r}_{2i}$
- (7) Computation of the root of the function  $f$ , Eq. (4) with polarimetric ray tracing, with Eq. (2). The solution gives the point  $P_2$
- (8) Computation of the thickness  $e$ , distance between  $Sl$  and  $P_2$ , and computation of the normal  $\vec{n}_2$

We have implemented [Fig. 5(a)] our approach with a partial Stokes polarimeter and an appropriate diffuse light source. We used a monochromatic Basler camera acA1300-30 gm,  $1280 \times 960$  pixels and a linear polarizer

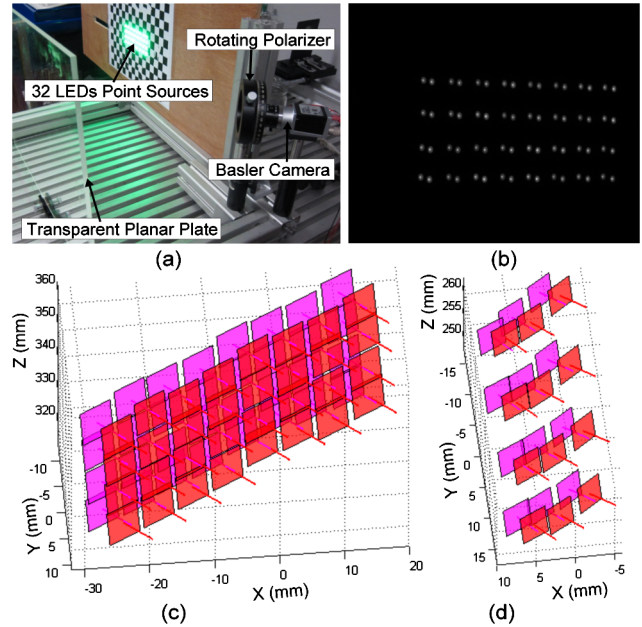


Fig. 5. Experimental results. (a) Our setup with a Plexiglas planar plate. (b) Image of the plate taken with the polarizer oriented at  $0^\circ$ . (c) Reconstruction result on the plate for each reconstructed points, tangent plane, and normal vector are plotted. (d) Reconstruction result on a Plexiglass cylinder.



(rotated manually). The lighting was an array of LEDs (which we consider as point light sources). We took three images (each one averaged 10 times to reduce noise) with the polarizer respectively oriented at  $0^\circ$ ,  $45^\circ$ , and  $90^\circ$ . The intensities were computed globally for each reflection, using a method derived from aperture photometry [17]. Figure 5 presents results obtained with a Plexiglas transparent planar plate of thickness 5 mm, and with a Plexiglass transparent cylinder of diameter 80 mm and thickness 3 mm. The reflection of the point sources on the two surfaces of the plate can be seen in Fig. 5(b) (acquired with the polarizer at  $0^\circ$ ). Figure 5(c) is the reconstruction result of the plate situated at about 35 cm from the camera, with 32 points for each face. The root-mean-square deviation of the measured normal vectors was  $0.14^\circ$  for both faces. We evaluated the error on the computed positions by fitting two planes on the results and by measuring the distance between the reconstructed point and these planes. The standard deviation of these distances was 0.63 mm for both faces, and the mean thickness was 4.98 mm. Figure 5(d) is a first reconstruction result obtained on the cylinder, with 12 points on each face. We took into account the curvature of the cylinder between points  $P_1$  and  $J$  to compute the refracted ray  $\vec{r}_{2t}$ . We fitted two cylinders on the results and computed the standard deviation of the distances with the two point clouds, which was 0.43 mm for the external surface, and 0.58 mm for the internal one. The mean measured thickness was 2.92 mm. We estimated that an error of  $0.05$  on degrees of polarization induces an error of  $0.1^\circ$  on the surfaces orientations and an error of 0.3 mm on their positions. When a small position error occurs on the external surface, it is reported on the internal one, so that the point  $P_2$  is shifted by the same error position, but the thickness stays almost the same.

In conclusion, the combination of shape from distortion and shape from polarization techniques is able to directly measure the position and orientation of both faces of a transparent object (assuming the two reflections are separated on the image) and a known refraction index. This approach, assuming only one surface is accessible, can be easily used in industry for surfaces and thickness inspection.

In future work, we plan to use the technique of [15] to deal with an angle greater than Brewster. A deeper study of the polarization state of the light coming from the internal surface could be also interesting in order to completely measure the orientation of this surface, even in non-coplanar cases. By doing so, we think we could use lines of light instead of points and then be able to acquire complete profiles of the objects. The density of the measure can also be improved by either using a controlled light source or moving the object in a scanning process. Finally we plan to relax the hypothesis about the local geometry of the external surface.

## References

1. I. Ihrke, K. N. Kutulakos, H. P. A. Lensch, M. Magnor, and W. Heidrich, in *STAR Eurographics* (2008).
2. A. C. Sanderson, L. E. Weiss, and S. K. Nayar, *IEEE Trans. Pattern Anal. Mach. Intell.* **10**, 44 (1988).
3. M. Tarini, H. P. A. Lensch, M. Goesele, and H.-P. Seidel, *Graph. Models* **67**, 233 (2005).
4. D. Miyazaki, M. Saito, Y. Sato, and K. Ikeuchi, *J. Opt. Soc. Am.* **19**, 687 (2002).
5. M. Ferraton, C. Stolz, and F. Mériaudeau, *Opt. Express* **17**, 21077 (2009).
6. N. J. W. Morris and K. N. Kutulakos, in *IEEE ICCV* (2007), pp. 1–8.
7. G. Wetzstein, D. Roodnick, W. Heidrich, and R. Raskar, in *IEEE ICCV* (2011), pp. 1180–1186.
8. K. N. Kutulakos and E. Steger, *Int. J. Comput. Vis.* **76**, 13 (2008).
9. B. Trifonov, D. Bradley, and W. Heidrich, in *Proc. Eurographics Symposium on Rendering* (2006), pp. 51–60.
10. M. B. Hullin, M. Fuchs, I. Ihrke, H.-P. Seidel, and H. P. A. Lensch, *ACM Trans. Graph.* **27**, 87 (2008).
11. M. Ben-Ezra and S. K. Nayar, in *IEEE ICCV*, vol. **2** (2003), pp. 1025–1032.
12. S. Savarese and P. Perona, in *ECCV*, vol. **2351** (2002), pp. 759–774.
13. R. Longhurst, *Optics*, 3rd ed. (Addison-Wesley, 1973).
14. M. Born and E. Wolf, *Principles of Optics* (Pergamon, 1959).
15. C. Stolz, M. Ferraton, and F. Mériaudeau, *Opt. Lett.* **37**, 4218 (2012).
16. G. Glaeser and H.-P. Schröcker, *J. Geom. Graph.* **4**, 1 (2000).
17. S. B. Howell, *Astronomical Society of the Pacific* **101**, 616 (1989).

## Queries

1. AU: Please provide the publisher name for the following Refs. [1], [6], [7], [9], [11], [12].